

Sensitivity analysis on chaotic dynamical system by Non-Intrusive Least Square Shadowing (NILSS)

Angxiu Ni^{a,*}, Qiqi Wang^a

^a*Aeronautics and Astronautics, MIT, 77 Mass Ave, Cambridge, MA 02139, USA*

Abstract

This paper develops the tangent Non-Intrusive Least Square Shadowing (NILSS) method, which computes the sensitivity for long-time averaged objectives in chaotic dynamical systems. In NILSS, we represent a tangent solution as a linear combination of a inhomogeneous tangent solution and some homogeneous tangent solutions. Then we solve a least square problem under this new representation. NILSS is easier to implement with existing solvers. Also, for chaotic systems with large degrees of freedom but a few unstable modes, NILSS has low computational cost. NILSS is applied to two chaotic PDE systems: the Lorenz 63 system, and a CFD simulation of a backward-facing step. In both cases, the sensitivities computed by NILSS reflect the trends in the objectives.

Keywords: Sensitivity analysis, linear response, tangent equation, chaos, dynamical systems, uniform hyperbolicity, ergodicity, least square shadowing

1. Introduction

Many important phenomena in engineering are chaotic. These include turbulent flows[1] and some fluid-structure interactions[2]. For these chaotic systems, we are often interested in long-time averaged quantities rather than instantaneous quantities. Furthermore, we want to perform sensitivity analysis, i.e. to know how the change in the parameters of the systems would affect those long-time averaged quantities. Such sensitivity analysis is the purpose of this paper.

Consider a deterministic dynamical system parameterized by s :

$$\frac{du}{dt} = f(u, s), \quad (1)$$

where $f(u, s) : \mathbb{R}^m \times \mathbb{R} \rightarrow \mathbb{R}^m$ is a smooth function, u is the state. A solution $u(t)$ is called the primal solution. The initial condition of the primal solution is denoted by $u(t=0) = u_0$.

*Corresponding author.

Email addresses: niangxiu@mit.edu (Angxiu Ni), qiqi@mit.edu (Qiqi Wang)

To define the objective, first let $J(u, s) : \mathbb{R}^m \times \mathbb{R} \rightarrow \mathbb{R}$ be a continuous function which defines the instantaneous objective. The averaged J over a time period of T is

$$\langle J \rangle_T := \frac{1}{T} \int_0^T J(u, s) dt. \quad (2)$$

$\langle J \rangle_T$ is a function of s , u_0 , and T . If we let T goes to infinity, then we obtain the objective of interest, $\langle J \rangle_\infty$, which is only determined by s and u_0 . Here we make the assumption of ergodicity [3], which means that u_0 does not affect $\langle J \rangle_\infty$. As a result, $\langle J \rangle_\infty$ is only a function of s .

We are interested in computing the sensitivity $d \langle J \rangle_\infty / ds$, since it is useful information in helping scientists and engineers design products [4, 5], control processes and systems [6, 7], solve inverse problems [8], estimate simulation errors [9, 10, 11], assimilate measurement data [12, 13] and quantify uncertainties [14].

When the dynamical system is chaotic, computing a meaningful $d \langle J \rangle_\infty / ds$ is challenging, since in general,

$$\frac{d}{ds} \langle J \rangle_\infty \neq \lim_{T \rightarrow \infty} \frac{\partial}{\partial s} \langle J \rangle_T (s, u_0, T). \quad (3)$$

That is, the process of $T \rightarrow \infty$ does not commute with differentiation with respect to s , if we fix u_0 [15]. As a result, the transient method, which is to apply conventional tangent method with a fixed u_0 , does not converge to the correct sensitivity. In fact, the transient method diverges most of the time for chaotic systems [15].

Many sensitivity analysis methods have been developed to compute $d \langle J \rangle_\infty / ds$. The conventional methods include the conventional finite difference method and the transient method. The ensemble method, developed by Lea et al[16, 17], computes the sensitivity by averaging $d \langle J \rangle_T / ds$ over an ensemble of trajectories. Another recent approach is based on the fluctuation dissipation theorem (FDT), as seen in [18, 19, 20, 21, 22, 23].

This paper follows the approach of Least Square Shadowing (LSS) developed by Wang, Hu and Blonigan [24, 14]. LSS first computes a bounded shift of a trajectory under an infinitesimal parameter change, which is called LSS solution. Then we can substitute the LSS solution into the derivative of Equation (2) to compute $d \langle J \rangle_\infty / ds$. LSS has been successfully applied to some dynamical systems such as the Lorenz 63 system and a modified Kuramoto-Sivashinsky equation[25, 14, 26]. LSS has also been applied by Blonigan et al. to sensitivity analysis for airfoils[15, 26]. It has been proved by Wang that under ergodicity and hyperbolicity assumptions, LSS converges to the correct sensitivity at a rate of $T^{-0.5}$, where T is the trajectory time length[24].

However, for large systems, LSS is expensive; it is also difficult to implement. In the original formulation of LSS, the majority of computation comes from solving a large linear system, the number of variables in which is the product of the dimension of the system and the number of time steps. As the system gets larger and trajectory longer, the linear system becomes very large

and possibly stiff. Although solving this linear system could be accelerated by preconditioning and iterative solvers [26], it would still be a large cost in both computer time and computer memory. Furthermore, previous formulations of LSS requires the Jacobian matrix $\partial_u f(u, s)$ at each time step. Many existing simulation software may not readily provide such information; thus modification to the code is required.

This paper presents the Non-Intrusive Least Square Shadowing (NILSS) method. The cost of NILSS is proportional to the number of unstable Lyapunov exponents. When this number is small, NILSS could be much cheaper than the conventional LSS. Another benefit is that NILSS does not require $\partial_u f(u, s)$. It does require the underlying tangent solver being able to start from any initial condition, whereas some existing solvers are coded only to perform integration from a zero initial condition. Nevertheless, it greatly reduces the amount of intrusion needed compared to the conventional LSS. When the number of unstable modes is small, NILSS stores less data than the conventional LSS. Furthermore, it allows storing most of its data onto hard drives instead of computer memory.

The rest of this paper is organized as follows: First, we examine the sensitivity with respect to parameters and initial conditions, and the relation between them. Then we explain the tangent NILSS method. Then we present a more detailed flowchart of the tangent NILSS algorithm on multiple time segments. Finally, we apply tangent NILSS to the Lorenz 63 system and a CFD simulation of a flow over a backward-facing step.

2. Connection between Sensitivity to initial conditions and parameters

Trajectories of chaotic dynamical systems depend sensitively on its parameters and initial conditions. The former means that by changing the parameters of the governing equation by a small amount, the new trajectory will grow further apart from the old one, even though they start from the same initial condition. This is similar to the latter sensitive dependence on initial conditions, which is better known as the ‘butterfly effects’. It means that for chaotic systems, a small difference in the initial condition can result in a large difference later on.

To illustrate the similarity between the two sensitivities, we use the example of the Lorenz 63 system, a simplified ODE model for atmospheric convection[27]. It has three states x, y, z and a parameter ρ . In Figure 1, we show the sensitive dependence of trajectories on both the initial condition and the parameter. In the left column, we plot on the x - z plane 1.8×10^7 trajectories with the same initial condition $u_0 = (12.00, 6.82, 36.47)$ but different ρ . Here ρ is uniformly distributed in $28 \pm \Delta\rho$, where $\Delta\rho = 1$: smaller ρ is indicated by colors with shorter wavelength (blue), while larger ρ by longer wavelength (red). On the right column, we plot the same number of trajectories with the same parameter $\rho = 28$ but their initial conditions are uniformly distributed in $u_0 \pm \Delta u_0$, where

$\Delta u_0 = [0.0939, -0.001053, 1.025]$. Here Δu_0 is chosen such that in the short time effect of changing initial conditions is similar to that of changing ρ .

There is much similarity and subtle differences between the effects of changing ρ and that of changing u_0 . As we can see in the first three rows in Figure 1, in the short time, changing ρ results in diverging trajectories which looks like the effect of only changing u_0 ; we call this the transient effect. In the long time, as shown in the last picture on the left, changing ρ results in a shifted attractor; we call this the long-time effect. To see that the attractor is shifted, notice that the last figure on the left has different colors in different parts: the upper rim is red, and the lower rim is blue. This is due to that the figure is the superposition of many attractors with different parameters. So the red shade on the upper rim indicates that as we increase ρ , the attractor moves upward in the z direction. This means that $\langle z \rangle_\infty$ may have a positive and well-defined sensitivity with respect to ρ .

The long-time effect of changing ρ is important for computing the long-time sensitivity, however, it is hidden under the diverging trajectories and is only visible after a long time and an ensemble of millions of trajectories. Our main goal in this paper, is to devise an algorithm such that we can ‘construct’ the transient effect and ‘subtract’ it from the effect of changing ρ , so that we can obtain the long-time sensitivity efficiently. In fact, in Figure 1, $\Delta u_0 = v\Delta\rho$, where v is the NILSS solution. As we shall see, this change in the initial condition give rise to the transient effect, which is subtracted from effect of changing ρ . We will clarify above qualitative description of ‘subtraction’ in later sections.

3. The idea of tangent NILSS

In this section we provide an explanation of tangent NILSS. First we mathematically describe the two effects of changing parameters, as described in the last section. To distill the long-time effect, we want to construct a homogeneous solution w which represents the transient effect, and subtract it from the effect of changing parameters. First we show that such w can be constructed as linear combination of unstable Characteristic Lyapunov Vectors (CLV), the coefficient of which is computationally expensive to find. Then we see how NILSS overcomes this difficulty by formulating such w from only the conventional tangent solution v^* and several homogeneous solutions $\{w_j\}$, where $\{w_j\}$ serves as an approximation of unstable CLVs. Finally, we look at how to compute $d\langle J \rangle_\infty / ds$ from these tangent solutions.

3.1. Extracting the long-time effect of a parameter perturbation

Now we mathematically analyze the effect of infinitesimal parameter and initial condition perturbations. From the analysis, we will derive a method to find an initial condition perturbation whose transient effect is similar to a given parameter perturbation. Using this initial condition perturbation, we can then subtract the transient effect from the parameter perturbation, thereby distilling the long-time effect of a parameter perturbation.

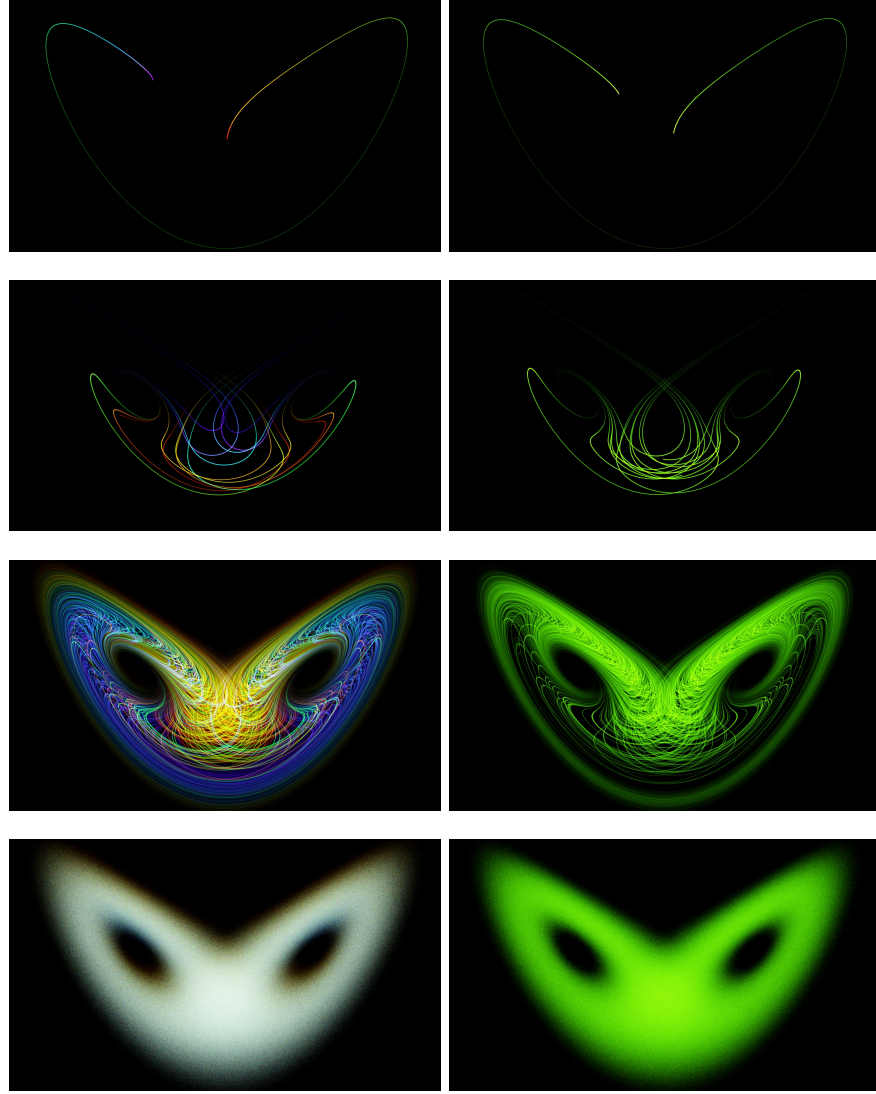


Figure 1: Snapshots of an ensemble of 1.8×10^7 trajectories of the Lorenz system, with ρ in the range [27,29], where smaller ρ is indicated by blue, larger ρ by red. Right column: trajectories with initial conditions around $(12.00, 6.82, 36.47)$, plus a random variable uniformly distributed in $\pm[0.0939, -0.001053, 1.025]$. From top to bottom: snapshots at time 1.67, 5.0, 10.0, and 41.67.

Assume the dynamical system in Equation (1) has an infinitesimal perturbation Δs in the parameter, the new parameter is $s + \Delta s$. The new solution is

denoted by $u + \Delta u$, which satisfy:

$$\frac{d(u + \Delta u)}{dt} = f(u + \Delta u, s + \Delta s). \quad (4)$$

Subtract by Equation (1) and neglect second order small quantities. Let $v = \Delta u / \Delta s$, since Δs is infinitesimal, $v = du/ds$. v satisfies the following inhomogeneous tangent equation:

$$\frac{dv}{dt} - \partial_u f v = \partial_s f, \quad (5)$$

where $\partial_u f$ is a $\mathbb{R}^m \times \mathbb{R}^m$ matrix and $\partial_s f$ is a \mathbb{R}^m column vector.

This v is undetermined unless an initial condition is specified. We denote v^* as the solution of Equation (5) with the initial condition $v^*(t = 0) = 0$. v^* is also the solution of the conventional tangent method, its zero initial condition reflect the assumption that u_0 is unchanged. Hence v^* characterizes the difference between infinitesimal different parameters, as shown in the left column of Figure 1.

If there is a small perturbation in u_0 but no perturbation in s , the new solution satisfies:

$$\frac{d(u + \Delta u)}{dt} = f(u + \Delta u, s). \quad (6)$$

Denote $w = du/ds$, it satisfies the homogeneous tangent equation:

$$\frac{dw}{dt} - \partial_u f w = 0. \quad (7)$$

To determine a particular w we should specify an initial condition. w characterizes the difference between infinitesimally different initial conditions, as shown in the right column of Figure 1.

Hence v^* and w describe the effect of changing s and u_0 , respectively. Also, Equation (7) differs from Equation (5) by setting the right hand side to zero. If two different tangent solutions, say v^* and an arbitrary v , both satisfies Equation (5), their difference is a homogeneous tangent solution w .

This matches our previous description: changing s has two effects, one is the same as changing u_0 , the other is shifting the attractor. Since we are interested in the latter, we want to find a w such that $v = v^* + w$ characterizes the motion of the attractor. Here we used addition, but we can replace w by $-w$ so that we have subtraction in the formula.

Subtracting such w from v^* is the main idea behind NILSS. The criterion of a desired v is that the magnitude of its orthogonal projection onto $V^\perp(u)$ is small. This allows us to compare states on the perturbed trajectory with states on the base trajectory, with them being close to each other. The more detailed reason for this criterion is described in Appendix C. Here $V^\perp(u)$ is defined as:

$$V^\perp(u) = \{v : v^T f(u) = 0\}. \quad (8)$$

The orthogonal projection v^\perp of v is defined as:

$$v^\perp = v - \frac{f^T v}{f^T f} f. \quad (9)$$

Similarly, we define w^\perp , Δu^\perp , $v^{*\perp}$, and later $\{\zeta_j^\perp\}$, corresponding to w , Δu , v^* and $\{\zeta_j\}$.

3.2. Constructing w from unstable Characteristic Lyapunov Vectors (CLV)

The main goal of NILSS is to find a w such that the magnitude of $v^\perp = v^{*\perp} + w^\perp$ is small. We should first be confirmed that a desired v exists. It is stated by the shadowing lemma [28] that the shadowing direction $v^\infty(u)$ has bounded $v^{\infty\perp}$ for all u on the attractor.

In this subsection, we shall see how to construct such a w , supposed that we could know v^∞ and all CLVs, which are homogeneous solutions. First, we can decompose $v^{*\perp} - v^{\infty\perp}$ into a linear combination of all CLVs; then w can be given by a linear combination of only the unstable CLVs. This method is unrealistic since it requires too much computation. Yet it is informative since it shows that we only need unstable CLVs to construct a desired w . Based on this knowledge, the NILSS method explained in the next subsection computes a desired w with only several homogeneous solutions, which serve as approximations of the unstable CLVs. The knowledge of LCVs and LEs introduced in this subsection is also useful for understanding NILSS.

To further clarify this method, we should first know what the Lyapunov Exponents (LE) and corresponding CLVs are. We assume that the dynamical system has a full set of LE and corresponding CLVs [29]. More specifically, there are $\{\lambda_j, j = 1, 2, \dots, m\}$, such that for any trajectory on the attractor and a corresponding homogeneous tangent solution $w(u)$, there is a unique representation of $w(u)$ by:

$$w(u) = \sum_{j=1}^m a_j \zeta_j(u), \quad (10)$$

where $a_j \in \mathbb{R}$ is a constant for all $u(t)$ on the trajectory.

Here each $\zeta_j(u)$ is a homogeneous tangent solution, and its magnitude behaves like an exponential function of time. That is, there exists $C_1, C_2 > 0$, such that for any $u(t)$ on the attractor and any j and t ,

$$C_1 e^{\lambda_j t} \|\zeta_j(u(0))\| \leq \|\zeta_j(u(t))\| \leq C_2 e^{\lambda_j t} \|\zeta_j(u(0))\|, \quad (11)$$

where $\{\lambda_j\}$ and $\{\zeta_j\}$ are LEs and CLVs, respectively. CLVs with $\lambda_j > 0$ are called unstable modes, those with negative $\lambda_j < 0$ are stable modes, and those with $\lambda_j = 0$ are neutral modes. Without loss of generality, we assume $\zeta_1, \dots, \zeta_{m_{us}}$ are unstable modes, ζ_m is the neutral mode, and the others are unstable modes. Unstable modes are the reason for ‘butterfly effect’, since a perturbation in the unstable subspace grows exponentially in time.

We assume that for all s we are interested in, there is no stagnation point close to the attractor Λ , and that Λ is bounded. These two assumptions imply

that, as justified in Appendix A, $f(u)$ is a CLV whose LE is 0. We further assume that $f(u)$ is the only neutral mode.

Although CLVs are not necessarily in V^\perp , we can project them onto V^\perp , now Equation (11) becomes:

$$w^\perp = \sum_{j=1}^m a_j \zeta_j^\perp(u), \quad (12)$$

where w^\perp and ζ_j^\perp are orthogonal projections as defined in Equation (9). Because V^\perp is perpendicular to $f(u)$, the projection of the neutral mode is zero. So the summation in Equation (12) is over only the stable and unstable modes, the total number of which is $m - 1$. Here we also call ζ_j^\perp stable or unstable modes based on their corresponding λ_j .

We assume that all CLVs are uniformly bounded away from each other. Under this assumption, the amplitudes of stable and unstable modes $\{\zeta_j^\perp\}$ also behave like exponentials, as defined in Equation 11. The justification of this claim is in Appendix B.

Suppose that we could know v^∞ and all CLVs. Since $v^\infty - v^*$ is a homogeneous tangent solution, we can decompose $v^{\infty\perp} - v^{*\perp}$ by Equation (12). With the same first m_{us} coefficients in this decomposition, Let

$$w = \sum_{j=1}^{m_{us}} a_j \zeta_j. \quad (13)$$

$v = v^* + w$ has small v^\perp , since $v^{\infty\perp} - v^{*\perp}$ is composed of only stable modes, which decay exponentially.

The important information in this method is that w is a linear combination of only the unstable modes. However, to find the coefficients of this linear combination, if we use the method given here, we need to know all the CLVs, as well as v^∞ . Not only the computational cost is high to find all CLVs, but also v^∞ is unknown a priori.

To improve the current method, we can use a linear combination of homogeneous solutions to approximate w . To achieve this, we first compute several homogeneous solutions $\{w_j\}$ with randomized initial conditions, the span of which can approximate the span of unstable CLVs. When determining the coefficients of the linear combination, to make v^\perp small, we directly minimize the norm of v^\perp in the affine space $v^{*\perp} + \text{span}\{w_j^\perp\}$. This improved procedure only requires v^* and $\{w_j\}$, and it leads to the NILSS method.

3.3. Computing bounded v^\perp by NILSS

This subsection presents the main part of NILSS, that is, how to find a $v = v^* + w$, such that the magnitude of v^\perp is small.

To do this, we minimize the L^2 norm of $v^\perp = v^{*\perp} + W^\perp a$:

$$\min_a \frac{1}{2} \int_0^T (v^{*\perp} + W^\perp a)^T (v^{*\perp} + W^\perp a) dt, \quad (14)$$

where v^* is the conventional tangent solution, and $W^\perp(t)$ is a matrix whose columns are homogeneous tangent solutions $\{w_j^\perp(t), j = 1, \dots, M\}$. The initial conditions $\{w_j(t=0)\}$ are randomized bounded vector in \mathbb{R}^m . The arguments for the optimization problem is $a \in \mathbb{R}^M$, with M being an integer larger than the number of positive LEs, m_{us} . The minimization in Equation (14) is the called NILSS problem on a single time segment, to distinguish it from the multiple time segments algorithm we will introduce in Section 4.

First we need to see that some a' can give a desired $v = v^* + Wa$. Because we are initializing $\{w_j^\perp\}$ randomly and $M \geq m_{us}$, there almost surely exists a' , such that $v^{\infty\perp} - (v^{*\perp} + W^\perp a')$ has no unstable modes. There might be stable modes left in this difference, but since stable modes decay exponentially,

$$(v^{*\perp} + W^\perp a') \approx v^{\infty\perp}. \quad (15)$$

Furthermore, due to the minimization, the magnitude of v^\perp is even smaller. Any $v^{*\perp} + W^\perp a$ contains a transient sensitivity component and a long-time sensitivity component. Because the transient component grows exponentially, a small $v^{*\perp} + W^\perp a$ on a long trajectory can not contain significant transient component [30, 24]. Hence the result v can be used to compute sensitivity. The intuition of the effect of minimization is illustrated in Figure 2.

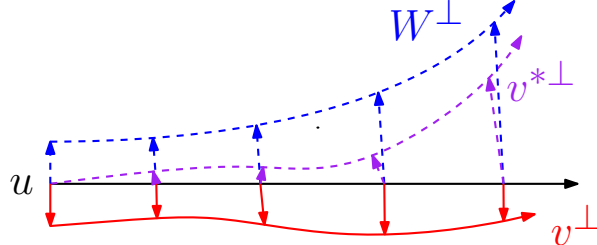


Figure 2: Intuition of NILSS: want to find a column vector a , such that the magnitude of $v^\perp = v^{*\perp} + W^\perp a$ is small.

The first benefit of NILSS is that it requires less modifications to existing tangent solvers. The data used in the NILSS problem are $v^{*\perp}$ and $\{w_j^\perp\}$. v^* is the result of the conventional tangent solver. $\{w_j\}$ can be computed by subtracting v^* from an inhomogeneous tangent solution v^w with nonzero initial condition. Assume the initial condition of a w_j is $w_j(0)$. To obtain w_j , first solve v^w by Equation (5) with initial condition $v^w(0) = w_j(0)$, then

$$w_j = v^w - v^*. \quad (16)$$

This way of computing w_j does not even require setting the right hand side in Equation (5) to be zero for conventional tangent solvers. Instead, we only require it being able to take arbitrary initial conditions, whereas conventionally zero initial conditions are assumed. Once we have v^* and $\{w_j\}$, $v^{*\perp}$ and $\{w_j^\perp\}$ can be computed by orthogonal projection onto $V^\perp(u)$, as shown in Equation (9).

The cost of NILSS is lower when the problem has fewer unstable modes. The optimization problem in NILSS is cheap to solve for small M , since there are only M arguments in the minimization problem posed in Equation (14). On the other hand, the main cost in NILSS is in preparing the optimization problem, that is, to compute $v^{*\perp}$ and $w_1^\perp(t), \dots, w_M^\perp(t)$. For problems with fewer unstable modes, there are fewer $\{w_j\}$ to compute.

A beneficial side-effect is that the total amount of data we need to store is less than that of the conventional LSS method. Furthermore, all the tangent solutions used in NILSS need not be put into computer memory at the same time. The formulation of NILSS allows us to put those tangent solutions on a hard drive, and read in two tangent solutions sequentially to compute their inner product. This implementation may reduce the computation speed, but saves much computer memory. Also, the optimization problem in Equation (14) is very small and requires little memory. To summarize, NILSS could potentially require much less computer memory than the conventional LSS.

3.4. Computing $d\langle J \rangle_\infty/ds$ from the tangent solution

Since $v - v^\perp$ is parallel to f , we can define

$$\xi f = v - v^\perp. \quad (17)$$

To find a pair (v^\perp, ξ) , first find a v which solves Equation (5), project v onto subspace V^\perp to find v^\perp , then use Equation (17) to find ξ .

Once we obtain v from solving an NILSS problem, we can compute the corresponding ξ . Then we have the following approximation for $d\langle J \rangle_\infty/ds$:

$$\frac{d\langle J \rangle_\infty}{ds} \approx \frac{1}{T} \left[\int_0^T (\partial_u f v^N + \partial_s J) dt + \xi|_0^T \langle J \rangle_T - (\xi J)|_0^T \right], \quad (18)$$

where $\langle J \rangle_T$ is as defined in Equation (2). Explanation of the above formula is in Appendix C.

A variant of tangent NILSS is the finite difference NILSS,¹ where we approximate tangent solutions by finite difference solutions. An explanation of finite difference NILSS could be found in Appendix D.

4. Tangent NILSS Algorithm

In this section, first we address numerical stability by rescaling $v^{*\perp}$ and W^\perp after every short segment of time ΔT . Then we discuss the criterion for determining the number of homogeneous solutions M , and segment length ΔT . Finally, we provide a detailed walk-through of the tangent NILSS algorithm.

¹The python package ‘fds’ which implements the algorithm introduced in this paper, both tangent NILSS and the finite difference variant, are available at github.com/qiqi/fds.

4.1. Solving NILSS on multiple time segments

Since both $v^{*\perp}$ and W^\perp grow exponentially, the round off error when storing them in the computer may become non-negligible. The growth in $v^{*\perp}$ and W^\perp will also make the covariance matrix $(W^\perp)^T W^\perp$ ill-conditioned, since all $\{w_j^\perp\}$ will eventually be dominated by the fastest growing unstable direction. This subsection shows how to prevent this by partitioning a long trajectory into several shorter segments.

We partition the time domain into K time segments $[t_0, t_1], [t_1, t_2], \dots, [t_{K-1}, t_K]$, with $t_0 = 0, t_K = T$. Define time segment i as $[t_i, t_{i+1}], i = 0, \dots, K-1$. On each time segment i , we define an inhomogeneous solution $\{v_i^*\}$ and homogeneous solutions $\{W_i\}$, with each $W_i = [w_{i,1}, \dots, w_{i,M}]$. The above notations is depicted in Figure 3.

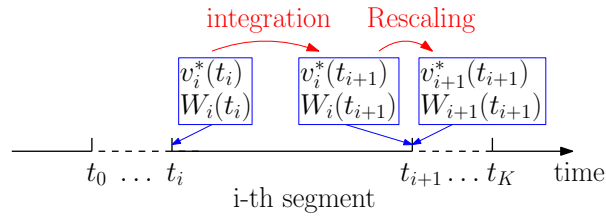


Figure 3: Notations used for NILSS, $t_0 = 0, t_K = T$

We want to rescale and orthogonalize $v_i^{*\perp}$ and W_i^\perp at the end of each segment so that they do not grow too large or too similar. We also want to keep the affine vector space $v^{*\perp} + \text{span}(W^\perp)$ the same across these segments, so that we can recover a continuous v^\perp :

$$v_i^{*\perp}(t_i) + \text{span}(W_i^\perp(t_i)) = v_{i-1}^{*\perp}(t_i) + \text{span}(W_{i-1}^\perp(t_i)), \quad (19)$$

where $\text{span}(W^\perp)$ is the vector space spanned by the column vectors of W^\perp .

To achieve this, we first orthonormalize W^\perp with a QR decomposition:

$$W_i^\perp(t_{i+1}) = Q_i R_i. \quad (20)$$

Set the initial conditions of the next tangent segment to

$$W_{i+1}(t_{i+1}) = Q_i. \quad (21)$$

In QR factorization, the column vectors in Q_i and W_i^\perp could represent each other if the column vectors in W_i^\perp are linearly independent. Indeed, the linear independence of the initial condition of W_i^\perp can be preserved after ΔT , if f is Lipschitz continuous. Hence $\text{span}(W_i^\perp(t_i)) = \text{span}(W_{i-1}^\perp(t_i))$.

We subtract from $v^{*\perp}$ its orthogonal projection on W^\perp to obtain the initial condition of the next time segment:

$$v_{i+1}^*(t_{i+1}) = v_i^{*\perp}(t_{i+1}) - W_{i+1}^\perp(t_{i+1}) b_i, \quad (22)$$

where $b_i = W_{i+1}^\perp(t_{i+1})^T v_i^{*\perp}(t_{i+1})$. $v_{i+1}^{*\perp}(t_{i+1})$ is still in the affine space $v_i^{*\perp}(t_i) + \text{span}(W_i^\perp(t_i))$. The magnitude of $v_i^{*\perp}(t_i)$ is reduced, since the unstable modes in it are subtracted through the projection.

We can recover a continuous v^\perp on the whole trajectory. Now Equation (19) is satisfied, for any a_{i-1} , there exists a_i such that:

$$v_i^{*\perp}(t_i) + W_i^\perp(t_i)a_i = v_{i-1}^{*\perp}(t_i) + W_{i-1}^\perp(t_i)a_{i-1}. \quad (23)$$

Hence we have the necessary condition to enforce the continuity requirement:

$$v_i^\perp(t_i) = v_{i-1}^\perp(t_i). \quad (24)$$

The solution v^\perp on multiple time segment is same as that of one longer segment. However, rescaling $v^{*\perp}$ and W^\perp at the end of each time segment prevents them from growing too large.

It is not a new idea of using QR factorization to rescale homogeneous solutions while keeping a continuous affine subspace. In a widely used technique for computing LE [31], the same idea was used.

4.2. Determining parameters for NILSS

There are two parameters in NILSS for users to decide: the number of homogeneous solutions M and the length of each time segment ΔT . This subsection discusses how to determine these parameters.

M is determined based on the Lyapunov Exponents (LE), which are byproducts of NILSS. According to [31], λ_j , the j -th largest LE is computed by:

$$\lambda_j \approx \frac{1}{K\Delta T} \sum_{i=1}^K |d_{i,j}|, \quad (25)$$

where $d_{i,j}$ is the j -th diagonal element in R_i .² Notice that the computation of $\{R_i\}$ only require W but not v^* . As we shall see in the detailed algorithm later, NILSS computes homogeneous solutions W before v^* . At the stage of computing W , we can gradually increase M and compute more LEs, until all positive LEs appear.

ΔT is determined by the constraint that the CLV with the largest LE do not dominate the M -th CLV. On each segment i , all $\{w_{i,j}^\perp(u(t)), 1 \leq j \leq M\}$ grow more and more parallel to the CLV with largest LE. If ΔT is large, the $W_i^\perp(t_{i+1})$ in Equation (20) and the covariance matrix C_i in Equation (29) will be ill-conditioned, which could pose a numerical problem for QR factorization in Equation (21) and for solving the NILSS problem in Equation (40). Assume the largest LE is λ_1 , and M -th largest LE is λ_M . The ratio between the magnitude of these two CLVs is:

$$\frac{\zeta_1(u(t))}{\zeta_M(u(t))} \approx \exp((\lambda_1 - \lambda_M)t). \quad (26)$$

²The python package ‘fds’ has a function which computes LEs.

We want to rescale W^\perp and $v^{*\perp}$ after time span $\Delta T \leq (\lambda_1 - \lambda_M)^{-1}$. This relation determines how we select ΔT .

Once we know how to determine parameters of NILSS, we can proceed to the detailed algorithm of NILSS.

4.3. Pre-process

First integrate Equation (1) for sufficient time before $t = 0$, so that u is on the attractor at the beginning of our algorithm. Then integrate Equation (1) from $t = 0$ to T to obtain the primal solution $u(t)$.

4.4. Computing the homogeneous solution $\{W_i\}$

We compute one inhomogeneous and M homogeneous tangent equations on each of the K time segments $[t_0, t_1], \dots, [t_{K-1}, t_K]$, with $t_0 = 0, t_K = T$. Time segment i is the range $[t_i, t_{i+1}]$. This notation is the same as that in Figure 3.

We start at the first segment with random initial conditions:

$$W_0(0) = [w_{0,1}(0), \dots, w_{0,M}(0)], \quad \text{with } w_{0,j}(0) \in V^\perp(u(0)). \quad (27)$$

Then proceed with the following algorithm starting at $i = 0$.

1. For each $j = 1, \dots, M$, starting from the initial conditions $\{w_{i,j}(t_i)\}$, Integrate Equation (7) to obtain $w_{i,j}(t), t \in [t_i, t_{i+1}]$. Through Equation (9), we compute the orthogonal projection onto V^\perp :

$$W_i^\perp(t) = [w_{i,1}^\perp(t), \dots, w_{i,M}^\perp(t)], \quad t \in [t_i, t_{i+1}]. \quad (28)$$

2. Compute and store

$$C_i = \int_{t_i}^{t_{i+1}} (W_i^\perp)^T W_i^\perp dt. \quad (29)$$

3. Orthonormalize $W_i^\perp(t_{i+1})$ with a QR decomposition:

$$W_i^\perp(t_{i+1}) = Q_i R_i. \quad (30)$$

Store R_i and set the initial conditions of the next segment to

$$W_{i+1}(t_{i+1}) = Q_i. \quad (31)$$

4. Let $i = i + 1$. Go to Step 1 unless $i = K$, in which case we proceed to Section 4.5.

Here we compute $\{w_{i,j}\}$ from Equation (7). They can as well be computed as the difference of two inhomogeneous tangent solutions:

$$\{w_{i,j}\} = v_{i,j}^w - v_i^0, \quad (32)$$

where $v_{i,j}^w$ has same initial condition as $w_{i,j}$, v_i^0 has zero initial condition at t_i .

4.5. Computing the inhomogeneous solution $\{v_i^*\}$

Start at the first time segment with initial condition: $v_0^*(0) = 0$, then proceed with the following algorithm starting at $i = 0$.

1. Starting from the initial condition $v_i^*(t_i)$, integrate the inhomogeneous Equation (5) to obtain $v_i^*(t)$, $t \in [t_i, t_{i+1}]$. Through Equation (9), we compute the orthogonal projection $v_i^{*\perp}(t)$, $t \in [t_i, t_{i+1}]$.

2. Compute and store

$$d_i = \int_{t_i}^{t_{i+1}} W_i^\perp{}^T v_i^{*\perp} dt. \quad (33)$$

3. Orthogonalize $v_i^{*\perp}(t_{i+1})$ with respect to $W_{i+1}^\perp(t_{i+1})$ to obtain the initial condition of the next time segment:

$$v_{i+1}^*(t_{i+1}) = v_i^{*\perp}(t_{i+1}) - W_{i+1}^\perp(t_{i+1})b_i, \quad (34)$$

where

$$b_i = W_{i+1}^\perp(t_{i+1})^T v_i^{*\perp}(t_{i+1}) \quad (35)$$

should be stored.

4. Let $i = i + 1$. Go to Step 1 unless $i = K$, in which case we proceed to Section 4.6.

Here we compute inhomogeneous solution v_i^* and homogeneous solution W_i separately. This way, we can first find all positive LEs by gradually increase M , since the computation of LE only requires homogeneous solutions. Once M is determined, we can go on to compute v^* . If we already know the number of positive LEs, then v_i^* and W_i can be computed simultaneously.

4.6. Computing v

Here we compute $\{v_i\}$ on each segment, with v_i^\perp continuous across different segments. The minimization objective in Equation (14) becomes:

$$\sum_{i=0}^{K-1} \int_{t_i}^{t_{i+1}} [(v_i^{*\perp})^T v_i^{*\perp} + 2(v_i^{*\perp})^T W_i^\perp a_i + a_i^T (W_i^\perp)^T W_i^\perp a_i] dt, \quad (36)$$

where $\{a_i \in \mathbb{R}^M, i = 0, \dots, K-1\}$. Other than a constant contribution from $(v_i^{*\perp})^T v_i^{*\perp}$, which is independent of $\{a_i\}$, we should choose $\{a_i\}$ by

$$\min_{\{a_i\}} \sum_{i=0}^{K-1} 2d_i^T a_i + a_i^T C_i a_i. \quad (37)$$

The continuity of v^\perp across t_i , the interface between segment $i-1$ and i , can be written as

$$v_{i-1}^{*\perp}(t_i) + W_{i-1}^\perp(t_i)a_{i-1} = v_i^{*\perp}(t_i) + W_i^\perp(t_i)a_i. \quad (38)$$

By applying Equation (30), (31), and (34), we can show this is equivalent to:

$$a_i = R_{i-1}a_{i-1} + b_{i-1}. \quad (39)$$

Combining the minimization problem in Equation (37) and the continuity constraints in Equation (39), we obtain the NILSS problem on multiple time segments:

$$\begin{aligned} \min_{\{a_i\}} \sum_{i=0}^{K-1} 2d_i^T a_i + a_i^T C_i a_i \\ \text{s.t. } a_i = R_{i-1}a_{i-1} + b_{i-1} \quad i = 1, \dots, K-1. \end{aligned} \quad (40)$$

Once $\{a_i\}$ is obtained by solving Equation (40), we can compute v_i within each time segment $t \in [t_i, t_{i+1}]$ by:

$$v_i(t) = v_i^*(t) + W_i(t)a_i. \quad (41)$$

4.7. Computing ξ_i

On each segment i , we define $\xi_i(t)$ by plugging v into Equation (17):

$$\xi_i f = v_i - v_i^\perp. \quad (42)$$

However, we only need to know the value of ξ_i at the beginning and end of each segment:

$$\begin{aligned} \xi_i(t_i) &= 0; \\ \xi_i(t_{i+1}) &= \frac{(v_i(t_{i+1}))^T f(u(t_{i+1}))}{f(u(t_{i+1}))^T f(u(t_{i+1}))} f(u(t_{i+1})). \end{aligned} \quad (43)$$

Here we used the fact that at the beginning of each segment, v_i^* and W_i are in V^\perp , hence so is v_i .

4.8. Computing $d\langle J \rangle_\infty / ds$

Once $v(t)$ is obtained, $d\langle J \rangle_\infty / ds$ is computed by

$$\frac{1}{T} \sum_{i=0}^{K-1} \int_{t_i}^{t_{i+1}} (\partial_u f v_i + \partial_s J) dt + \xi_i(t_{i+1})(\langle J \rangle_T - J(T)). \quad (44)$$

The derivation of Equation (44) from Equation (18) is in Appendix E.

Alternatively, the sensitivity can be computed without explicitly forming $\{v_i(t)\}$. The sensitivity contribution of $\{v_i(t)\}$ within each time interval can be computed from v_i^* and $w_{i,j}$ when they are solved, and a linear combination of them, with a_i being the coefficients.

5. Numerical Results on Lorenz attractor

We apply the tangent NILSS to the Lorenz 63 system. It has three states x, y, z , so $m = 3$. The governing equation is:

$$\frac{dx}{dt} = \sigma(y - x), \quad \frac{dy}{dt} = x(\rho - z) - y, \quad \frac{dz}{dt} = xy - \beta z. \quad (45)$$

In our current numerical example, we set $\sigma = 10, \beta = 8/3$.

The parameter of the system is ρ , which varies in range $[2, 45]$. The Lorenz 63 system has different behaviors when ρ changes [32]:

- $2 \leq \rho < 24.7$, two fixed point attractors.
- $24.7 \leq \rho < 31$, one quasi-hyperbolic strange attractor.
- $31 \leq \rho \leq 45$, one non-hyperbolic attractor.

For our study, we select the objective to be:

$$\langle J \rangle_\infty = \lim_{T \rightarrow \infty} \frac{1}{T} \int_0^T z \, dt. \quad (46)$$

We use $\langle J \rangle_{T'}$ to approximate $\langle J \rangle_\infty$, where $T' = 100$ time units. Notice that in general T' is not necessarily equal to the length of trajectory on which we perform NILSS, T .

When solving the primal solution $u = (x, y, z)^T$, we use Euler forward integration with time step size 0.005. Each segment has 1000 steps, that is, 5 time units. We perform NILSS over $K = 20$ segments, that is, $T = 100$ time units.

The LEs of Lorenz 63 system should satisfy the following constraints [33]:

$$\begin{aligned} \lambda_1 + \lambda_2 + \lambda_3 &= -(1 + \sigma + \beta); \\ \lambda_2 &= 0. \end{aligned} \quad (47)$$

Here λ_2 is the LE whose corresponding CLV is parallel to du/dt . Since $\lambda_1 + \lambda_3 < 0$, there are at most 1 positive LE. Hence we set the number of homogeneous solutions to be $M = 1$.

With above setting, we compute $\langle J \rangle_\infty$ and $d \langle J \rangle_\infty / d\rho$. The result is shown in Figure 4 and Figure 5. It can be observed from Figure 4 that the true value of $d \langle J \rangle_\infty / d\rho$ is about 1 for all ρ . The sensitivities computed with NILSS match this observation.

6. Numerical Results on CFD Simulation of flow over a backward-facing step

We apply NILSS to a chaotic flow over a backward-facing step. Specifically, we use the same geometry and mesh as in the PitzDaily tutorial of OpenFOAM

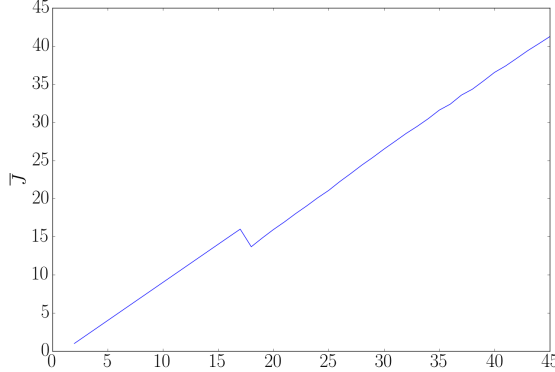


Figure 4: Averaged objective $\langle J \rangle_\infty$ vs. parameter ρ for the Lorenz 63 system, with $\sigma = 10, \beta = 8/3$. $\langle J \rangle_\infty$ is approximated by $\langle J \rangle_{T'}$, which is averaged over $T' = 100$ time units.

4.0, which is modeled from the experiment by Pitz and Daily [34]. This problem is a two-dimensional flow over a backward-facing step near the inlet and a contracting nozzle at the outlet. The geometry is shown in Figure 6.

For the numerical simulation, we use OpenFOAM 4.0 as the solver. We use the mesh as provided in the tutorial: there are 12225 cells, which is shown in Figure 7. Specifically, we solve incompressible Navier-Stokes equation by pisoFOAM. We use 2nd order finite volume scheme; the time-integration method is PISO (Pressure Implicit with Splitting of Operator), time step size is 1×10^{-5} second. We use dynamic one equation eddy-viscosity model for turbulence model [35]. The viscosity is $1 \times 10^{-5} m^2/s$.

We set no-slip wall condition for all boundaries except for the inlet and outlet. The velocity at the inlet boundary takes a uniform fixed value in the x-direction, the magnitude of which is the parameter of this problem. For the base case, we set inlet velocity $U = (10, 0, 0) m/s$. For the outlet, we use the ‘inletOutlet’ option, which is to switch between the zero value and the zero gradient boundary condition, depending on the flow direction.

With above settings, a typical snapshot of the flow field is shown in Figure 8. The flow is chaotic but not turbulent, since it is two-dimensional.

The parameter in this problem is the x-directional velocity at the inlet, U_{x0} . We use four different objectives: the long-time average of $U_x/10$, $(U_x/10)^2$, $(U_x/10)^4$, and $(U_x/10)^8$. Here U_x is the x-direction velocity at a probe at coordinate (50.8mm, 25.3mm). The location of the probe is very close to the upper surface, as shown in Figure 8.

The objective $\langle J \rangle_\infty$ is approximated by $\langle J \rangle_{T'}$ averaged over 2×10^5 time steps, that is, $T' = 2$ seconds. To get the uncertainty of the objective, we divide the simulation into 5 equally long parts, and average the objective over each part. Denote these averaged objectives by J_1, \dots, J_5 , the corrected sample

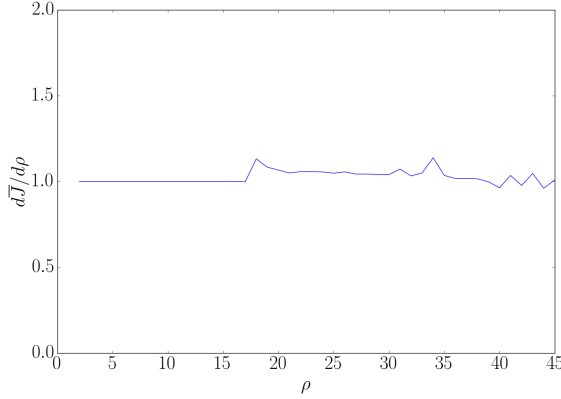


Figure 5: $d\langle J \rangle_\infty / d\rho$ computed for each ρ by the tangent NILSS. The time length of trajectories is $T = 100$, which is partitioned into 20 segments of length 5. NILSS uses one homogeneous tangent solutions.



Figure 6: Geometry used in the simulation of a chaotic flow over a backward-facing step, dimensions in mm. All boundaries except inlet/outlet are solid walls.

standard deviation between them are:

$$\sigma' = \sqrt{\frac{1}{4} \sum_{k=1}^5 (J_k - \langle J \rangle_{T'})^2}. \quad (48)$$

Here we assume that the standard deviation is inverse proportional to the square root of time length, so we use $\sigma = \sigma' / \sqrt{5}$ as the standard deviation of $\langle J \rangle_{T'}$. We further assume that, when averaging over random trajectories, the distribution of $\langle J \rangle_{T'}$ is Gaussian, hence $\pm 2\sigma$ gives its 95% confidence interval. Objectives for difference parameters in range [9,11] are shown in the right column of Figure 10, where the bars indicate the 95% confidence interval.

For NILSS, we use finite difference to approximate tangent solutions, as explained in Appendix D. Each segment has 250 time steps, that is, 0.0025

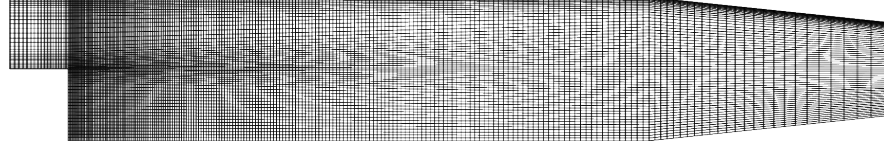


Figure 7: Mesh of test case, as provided in the tutorial of OpenFOAM 4.0

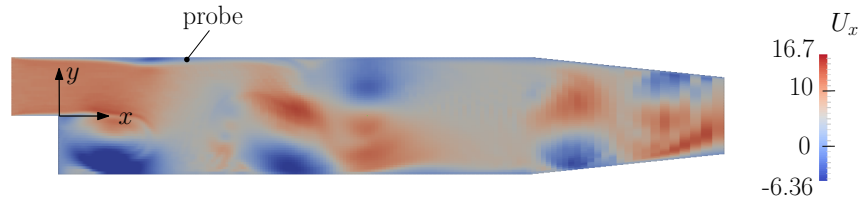


Figure 8: Flow field at time 0.091. Plotted by x-directional velocity U_x .

second. To compute the sensitivity, we run NILSS over $K = 200$ segments, that is, $T = 0.5$ second.

To determine the number of homogeneous solutions, M , we compute LEs by the method described in section 4.2. For a particular LE, denoted by λ , its computed value changes with the length of the trajectory, or equivalently, the number of segments, i . We use λ_i to denote its value computed using data from segments $1, 2, \dots, i$. To determine the uncertainty in LEs computed, we compute the smallest interval that converges at rate $i^{-0.5}$ and contains all $\{\lambda_i\}$. More specifically, we assume that $\{\lambda_i\}$ converges to some λ_0 as we increase i , and its confidence interval is proportional to $i^{-0.5}$. To find λ_0 , first define $C(\lambda)$ as:

$$C(\lambda) = \min\{C' \mid |\lambda - \lambda_i| \leq C'i^{-0.5}, \text{ for all } i \leq K\}, \quad (49)$$

where K is the number of segments. We define λ_0 as such that the corresponding $C(\lambda_0)$ is smallest:

$$\lambda_0 = \arg \min_{\lambda} \{C(\lambda)\}. \quad (50)$$

We regard $CK^{-0.5}$ as the confidence interval for λ_0 . The convergence history of the largest 16 LEs are shown in the left of Figure 9. The λ_0 and confidence intervals for each LE are shown in the right of Figure 9. As can be observed, the total number of positive LEs is smaller than 16. So we set $M = 16$.

With above settings, the cost of NILSS is proportional to the total time steps computed, which is $200 \times 250 \times 18 = 9 \times 10^5$. Here 18 is the number of trajectories computed. We need one v^* and 16 $\{w_j\}$, that is 17 tangent solutions in total. Each tangent solution requires the finite difference between a base solution and a perturbed solution to approximate. These finite differences

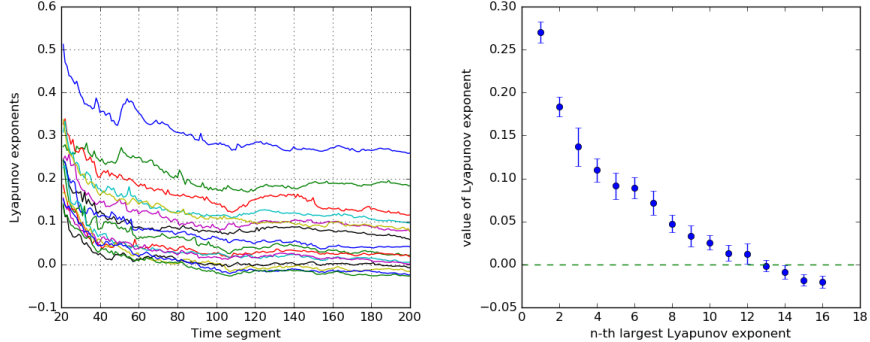


Figure 9: Lyapunov exponents (LE). Left: convergence history of 16 different LEs as the trajectory length increased, where the trajectory length is represented by the number of segments. Right: confidence interval of the largest 16 LEs.

use the same base solution, so we compute one base solution and 17 perturbed solutions, each with 200×250 time steps in primal solution.

We want to give confidence intervals for the sensitivities computed by NILSS. Similar to the case of LE, the value of dJ/ds changes with T , or equivalently, the number of segments. We use $(dJ/ds)_i$ to denote the sensitivity computed using data from segments $1, 2, \dots, i$. Here we assume that $\{(dJ/ds)_i\}$ converges to some $(dJ/ds)_0$ as we increase i , and its confidence interval is proportional to $i^{-0.5}$. To find $(dJ/ds)_0$, first define $C(dJ/ds)$ as:

$$C\left(\frac{dJ}{ds}\right) = \min \left\{ C' \mid \left| \frac{dJ}{ds} - \left(\frac{dJ}{ds} s \right)_i \right| \leq C' i^{-0.5}, \text{ for all } i \leq K \right\}. \quad (51)$$

We define $(dJ/ds)_0$ as such that the corresponding $C((dJ/ds)_0)$ is smallest:

$$\left(\frac{dJ}{ds} \right)_0 = \arg \min_{dJ/ds} \left\{ C\left(\frac{dJ}{ds}\right) \right\}. \quad (52)$$

We regard $CK^{-0.5}$ as the confidence interval for $(dJ/ds)_0$. The left column in Figure 10 is a log-log plot of $| (dJ/ds)_0 - (dJ/ds)_i |$ for $U_{x0} = 10$, where the lines indicate $Ci^{-0.5}$. Similarly, we find the confidence interval of the sensitivity at $U_{x0} = 11$. In the right column of Figure 10, the wedges indicate these confidence intervals of sensitivities. As we can see, the sensitivities computed by NILSS correctly reflect the trend in long-time averaged objectives.

In our current example, the cost of the NILSS is roughly the same as that of the conventional finite difference method. For chaotic systems, with fixed u_0 and T' , the relation $\langle J \rangle_{T'} \sim s$ has many local fluctuations [14]. To smoothen out these local fluctuations in the conventional finite difference method, we do a linear regression over 5 parameters in [9,11]; the total number of time steps computed in primal solutions is $5 \times 2 \times 10^5 = 1 \times 10^6$. In NILSS, the total

number of time steps in primal solutions is 9×10^5 . This forms the major cost of the finite difference NILSS, which is roughly the same as the conventional finite difference method.

However, here we may be making a comparison in favor of the conventional finite difference. In Figure 10, the range span of parameters is 2; it is too large for the last two objectives, since the relations between objectives and parameters are not linear. In these cases, if we want to reduce the error in linearly approximating a nonlinear function, the parameters range should be smaller. However, this requires the confidence intervals of objectives also be reduced. Otherwise, the uncertainties in objectives are divided by a smaller parameter range: this would give rise to a larger uncertainty in the sensitivity. To obtain smaller confidence intervals of objectives, we require longer trajectories, which means larger computational cost for the conventional finite difference method.

When there are multiple parameters, the cost of NILSS is even lower than the conventional finite difference method. For tangent NILSS, Equation (5) has right hand side $\partial_s f$, which says v^* would change if we have a new parameter. However, w_j does not depend on the parameter s , so they could be reused for the new parameter. The marginal cost for a new parameter is only to compute a new v^* . In our finite difference NILSS for this problem, 18 trajectories were computed, one is base trajectory, one is with perturbed parameter but same initial condition, 16 are with perturbed initial condition but same parameter. Only the one with perturbed parameter should be recomputed for a new choice of parameter. So the marginal cost of another parameter is only 1/18 of the cost of the first parameter. On the other hand, for the conventional finite difference, 5 trajectories are computed, one is base trajectory, 4 are with perturbed parameters. As a result, 4 trajectories should be recomputed for a new choice of parameter. This means the marginal cost of another parameter is 4/5 of the cost of the first parameter, which is higher than that of finite difference NILSS.

The cost of NILSS is likely lower than that of the conventional LSS method. The number of states in our problem is $12225 \times 3 = 36675$. If we perform the conventional LSS on a same time span of 5×10^4 steps, it would require solving a linear equation system with 1.8×10^9 variables. This would be a very large cost in both computation time and computer storage.

7. Conclusions

The Non-Intrusive Least Square Shadowing (NILSS) is a method which computes the sensitivity of long-time averaged objectives in chaotic systems. NILSS is a variant of the Least Square Shadowing (LSS) method [14], but it has several advantages over the conventional LSS method:

1. It potentially requires only minor modifications to existing solvers.
2. For problems with a few unstable modes, which is the case for many engineering applications, NILSS has lower computational cost.
3. NILSS requires less computer memory.

NILSS has been demonstrated on the Lorenz 63 system and a CFD simulation for a flow over a backward-facing step. In both cases, the sensitivities given by NILSS can reflect the trend between objectives and parameters. For the latter case, NILSS has a similar computational cost as the conventional finite difference method. We further argued that NILSS would be cheaper than the conventional finite difference, if the relation between objectives and parameters is nonlinear, or if we are interested in multiple parameters. It is also verified that the latter test case has a low-dimensional attractor, with less than 16 positive Lyapunov exponents.

References

References

- [1] A. N. Kolmogorov, The Local Structure of Turbulence in Incompressible Viscous Fluid for Very Large Reynolds Numbers, *Proceedings: Mathematical and Physical Sciences* 434 (1890) (1991) 9–13.
URL <http://www.jstor.org/stable/51980>
- [2] E. Dowell, Flutter of a buckled plate as an example of chaotic motion of a deterministic autonomous system, *Journal of Sound and Vibration* (1982) 333–344.
URL <http://www.sciencedirect.com/science/article/pii/0022460X82902590>
- [3] P. Walters, An introduction to ergodic theory, Vol. 79, Springer Science & Business Media, 2000.
- [4] A. Jameson, Aerodynamic design via control theory, *Journal of scientific computing* 3 (3) (1988) 233–260.
- [5] J. J. Reuther, A. Jameson, J. J. Alonso, M. J. Rimllnger, D. Saunders, Constrained Multipoint Aerodynamic Shape Optimization Using an Adjoint Formulation and Parallel Computers, Part 2, *Journal of Aircraft* 36 (1) (1999) 61–74. doi:10.2514/2.2414.
URL <http://arc.aiaa.org/doi/abs/10.2514/2.2414>
- [6] T. R. Bewley, Flow control: new challenges for a new Renaissance, *Progress in Aerospace Sciences* 37 (2001) 21–58.
URL <http://turbulence.ucsd.edu>.
- [7] T. R. Bewley, P. Moin, R. Temam, DNS-based predictive control of turbulence: an optimal benchmark for feedback algorithms, *Journal of Fluid Mechanics* 447 (2001) 179–225. doi:10.1017/S0022112001005821.
- [8] J. Tromp, C. Tape, Q. Liu, Seismic tomography, adjoint methods, time reversal and banana-doughnut kernels, *Geophys. J. Int.* doi:10.1111/j.1365-246X.2004.02453.x.

[9] R. Becker, R. Rannacher, An optimal control approach to a posteriori error estimation in finite element methods, *Acta Numerica* 10. doi:10.1017/S0962492901000010.
 URL http://www.journals.cambridge.org/abstract_S0962492901000010

[10] M. B. Giles, E. Süli, Adjoint methods for PDEs: a posteriori error analysis and postprocessing by duality, *Acta Numerica* 11. doi:10.1017/S096249290200003X.
 URL http://www.journals.cambridge.org/abstract_S096249290200003X

[11] K. J. Fidkowski, D. L. Darmofal, Review of Output-Based Error Estimation and Mesh Adaptation in Computational Fluid Dynamics doi:10.2514/1.J050073.

[12] J.-N. Thepaut, P. Courtier, Four-dimensional variational data assimilation using the adjoint of a multilevel primitive-equation model, *Quarterly Journal of the Royal Meteorological Society* 117 (502) (1991) 1225–1254. doi:10.1002/qj.49711750206.
 URL <http://doi.wiley.com/10.1002/qj.49711750206>

[13] P. Courtier, J. Derber, R. Errico, J. Louis, T. Vukićević, Important literature on the use of adjoint, variational methods and the Kalman filter in meteorology (oct 1993). doi:10.1034/j.1600-0870.1993.t01-4-00002.x.
 URL <http://tellusa.net/index.php/tellusa/article/view/14898> [http://onlinelibrary.wiley.com/doi/10.1034/j.1600-0870.1993.t01-4-00002.x/abstract\\$&delimiter](http://onlinelibrary.wiley.com/doi/10.1034/j.1600-0870.1993.t01-4-00002.x/abstract$&delimiter) <http://www.blackwell-synergy.com/doi/abs/10.1034/j.1600-0870.1993.t01-4-00002.x>

[14] Q. Wang, R. Hu, P. Blonigan, Least Squares Shadowing sensitivity analysis of chaotic limit cycle oscillations, *Journal of Computational Physics* 267 (2014) 210–224.

[15] P. J. Blonigan, Q. Wang, E. J. Nielsen, B. Diskin, Least Squares Shadowing Sensitivity Analysis of Chaotic Flow around a Two-Dimensional Airfoil, in: 54th AIAA Aerospace Sciences Meeting, no. January, 2016, pp. 1–28. doi:10.2514/6.2016-0296.
 URL <http://arc.aiaa.org/doi/10.2514/6.2016-0296>

[16] D. J. Lea, M. R. Allen, T. W. N. Haine, Sensitivity analysis of the climate of a chaotic system, *Tellus Series a-Dynamic Meteorology and Oceanography* 52 (5) (2000) 523–532. doi:10.1256/qj.01.180.

[17] G. L. Eyink, T. W. N. Haine, D. J. Lea, Ruelle's linear response formula, ensemble adjoint schemes and Lévy flights, *Nonlinearity* 17 (5) (2004) 1867.

[18] J. Thuburn, Climate sensitivities via a FokkerPlanck adjoint approach, *Quarterly Journal of the Royal Meteorological Society* 131 (605) (2005) 73–92. doi:10.1256/qj.04.46.
URL <http://doi.wiley.com/10.1256/qj.04.46>

[19] T. N. Palmer, A nonlinear dynamical perspective on model error: A proposal for non-local stochastic-dynamic parametrization in weather and climate prediction models, *Quarterly Journal of the Royal Meteorological Society* 127 (572) (2001) 279–304. doi:10.1002/qj.49712757202.
URL <http://doi.wiley.com/10.1002/qj.49712757202>

[20] L.-S. Young, What are SRB measures, and which dynamical systems have them?, *Journal of Statistical Physics* 108 (5) (2002) 733–754.

[21] C. E. Leith, Climate Response and Fluctuation Dissipation, *Journal of the Atmospheric Sciences* 32 (10) (1975) 2022–2026. doi:10.1175/1520-0469(1975)032<2022:CRAFD>2.0.CO;2.
URL [http://journals.ametsoc.org/doi/abs/10.1175/1520-0469\(1975\)032<2022:CRAFD>2.0.CO;2](http://journals.ametsoc.org/doi/abs/10.1175/1520-0469(1975)032<2022:CRAFD>2.0.CO;2)

[22] R. V. Abramov, A. J. Majda, Blended response algorithms for linear fluctuation-dissipation for complex nonlinear dynamical systems, *Nonlinearity* 20 (12) (2007) 2793.

[23] R. V. Abramov, A. J. Majda, New Approximations and Tests of Linear Fluctuation-Response for Chaotic Nonlinear Forced-Dissipative Dynamical Systems, *Journal of Nonlinear Science* 18 (3) (2008) 303–341. doi:10.1007/s00332-007-9011-9.
URL <http://link.springer.com/10.1007/s00332-007-9011-9>

[24] Q. Wang, Convergence of the Least Squares Shadowing Method for Computing Derivative of Ergodic Averages, *SIAM Journal on Numerical Analysis* 52 (1) (2014) 156–170. arXiv:arXiv:1304.3635v7, doi:10.1137/130917065.
URL <http://pubs.siam.org/doi/abs/10.1137/130917065>

[25] P. Blonigan, S. Gomez, Q. Wang, Least Squares Shadowing for sensitivity analysis of turbulent fluid flows, in: 52nd Aerospace Sciences Meeting, 2014, pp. 1–24. arXiv:1401.4163.
URL <http://arxiv.org/abs/1401.4163>

[26] P. J. Blonigan, Least Squares Shadowing for Sensitivity Analysis of Large Chaotic Systems and Fluid Flows, Ph.d thesis, MIT (2016).

[27] E. N. Lorenz, Deterministic Nonperiodic Flow, *Journal of the Atmospheric Sciences* 20 (2) (1963) 130–141. doi:10.1175/1520-0469(1963)

020<0130:DNF>2.0.CO;2.
 URL [http://journals.ametsoc.org/doi/abs/10.1175/1520-0469\(2013\)281963](http://journals.ametsoc.org/doi/abs/10.1175/1520-0469(2013)281963)

[28] S. Y. Pilyugin, Shadowing in Dynamical Systems, Lecture Notes in Mathematics. doi:10.1007/BFb0093184.

[29] D. Ruelle, Ergodic theory of differentiable dynamical systems, Publications Mathématiques de l’Institut des Hautes Études Scientifiques 50 (1) (1979) 27–58. doi:10.1007/BF02684768.
 URL <http://dx.doi.org/10.1007/BF02684768>

[30] M. Chater, A. Ni, P. J. Blonigan, Q. Wang, Least Squares Shadowing method for sensitivity analysis of differential equations, submitted to SIAM Journal on Numerical Analysis, arXiv:1509.02882arXiv:1509.02882.
 URL <http://arxiv.org/abs/1509.02882>

[31] G. Benettin, L. Galgani, A. Giorgilli, J.-M. Strelcyn, Lyapunov Characteristic Exponents for smooth dynamical systems and for hamiltonian systems; A method for computing all of them. Part 2: Numerical application, Mecanica 15 (1) (1980) 21–30. doi:10.1007/BF02128237.
 URL <http://dx.doi.org/10.1007/BF02128237>

[32] C. Sparrow, The Lorenz equations: bifurcations, chaos, and strange attractors, Vol. 41, Springer Science & Business Media, 2012.

[33] J. Bovy, Lyapunov exponents and strange attractors in discrete and continuous dynamical systems, Tech. rep., KU Leuven University, Theoretical Physics Project (2004).

[34] R. W. Pitz, J. Daily, Combustion in a turbulent mixing layer formed at a rearward facing step, AIAA Journal 21 (11) (1983) 1565–1570.

[35] W.-W. Kim, S. Menon, A new dynamic one-equation subgrid-scale model for large eddy simulations, in: AIAA, 33 rd Aerospace Sciences Meeting and Exhibit, Reno, NV, 1995.

Appendix A. Showing $f(u)$ is a CLV with zero LE

We assume that there is no stagnation point close to the attractor Λ , and that Λ is bounded. The first assumption means that there is a positive lower bound for $f(u)$, i.e. there exists $C_1^0 > 0$, such that

$$\|f(u)\| \geq C_1^0, \quad \text{for all } u \in \Lambda. \quad (\text{A.1})$$

Since $f(u, s)$ is a continuous function, $f(u)$ is continuous for fixed s . Together with the second assumption, we see that the $f(\Lambda)$ is bounded, i.e. there exists $C_2^0 > 0$, such that

$$\|f(u)\| \leq C_2^0, \quad \text{for all } u \in \Lambda. \quad (\text{A.2})$$

We check that for a fixed s , $f(u)$ is a homogeneous tangent solution. Indeed,

$$\frac{df(u)}{dt} = \frac{\partial f}{\partial u} \frac{du}{dt} = \partial_u f f. \quad (\text{A.3})$$

Where the last equality is due to Equation (1).

Denote $C_1 = C_1^0/\|f(u(0))\|$, $C_2 = C_2^0/\|f(u(0))\|$, then $f(u)$ is a CLV whose LE is 0, since

$$C_1 e^{0t} \|f(u(0))\| \leq \|f(u(t))\| \leq C_2 e^{0t} \|f(u(0))\|. \quad (\text{A.4})$$

Which satisfies Equation (11).

Appendix B. Property of $\{\zeta_j^\perp\}$

Here we show that the amplitudes of stable and unstable modes, $\{\zeta_j^\perp\}$, behave like exponentials.

We assume that all CLVs are uniformly bounded away from each other. First define the angle $\alpha_{ij}(u)$ between two CLVs,

$$\alpha_{ij}(u) = \arccos \frac{\zeta_j(u)^T \zeta_j(u)}{\|\zeta_j(u)\| \|\zeta_j(u)\|}, \quad i \neq j. \quad (\text{B.1})$$

The assumption means that there is $\alpha_0 > 0$ such that:

$$\alpha_{ij}(u) > \alpha_0, \quad \text{for all } i \neq j, u \in \Lambda. \quad (\text{B.2})$$

Where Λ is the attractor.

Since $f(u)$ is also a CLV, the angle between $\{\zeta_j\}$ and $f(u)$ is greater than α_0 , the angle between $\{\zeta_j\}$ and V^\perp is always smaller than $\pi/2 - \alpha_0$. Hence,

$$\|\zeta_j^\perp(u(t))\| \geq \sin(\alpha_0) \|\zeta_j(u(t))\| \geq \sin(\alpha_0) e^{\lambda_j t} C_1 \|\zeta_j(u(0))\| \geq C'_1 e^{\lambda_j t} \|\zeta_j^\perp(u(0))\|. \quad (\text{B.3})$$

Here $C'_1 = \sin(\alpha_0) C_1$. On the other hand,

$$\|\zeta_j^\perp(u(t))\| \leq \|\zeta_j(u(t))\| \leq C_2 e^{\lambda_j t} \|\zeta_j(u(0))\| \leq C'_2 e^{\lambda_j t} \|\zeta_j^\perp(u(0))\|. \quad (\text{B.4})$$

Here $C'_2 = \sin(\alpha_0) C_2$. To summarize, there is $C'_1, C'_2 > 0$, such that

$$C'_1 e^{\lambda_j t} \|\zeta_j^\perp(u(0))\| \leq \|\zeta_j^\perp(u(t))\| \leq C'_2 e^{\lambda_j t} \|\zeta_j^\perp(u(0))\|. \quad (\text{B.5})$$

Here all $\lambda_j \neq 0$ since they correspond to stable or unstable modes.

Appendix C. Derivation of $d\langle J \rangle_\infty/ds$

With a perturbation in s , the governing equation for u is:

$$\frac{d(u + \Delta u)}{dt} = f(u + \Delta u, s + \Delta s). \quad (\text{C.1})$$

We define another quantity, η . As shown in fig C.11, assume that at time t , the difference of the new trajectory from the original one is $\Delta u^\perp(t)$. After Δt , neglecting higher order small quantities, this difference becomes

$$\Delta u(t + \Delta t) = \Delta u^\perp(t) + (\partial_u f \Delta u^\perp(t) + \partial_s f \Delta s) \Delta t. \quad (\text{C.2})$$

The projection of $\Delta u(t + \Delta t)$ onto V^\perp is denoted by $\Delta u^\perp(t + \Delta t)$, as in Equation (9). The projection onto the direction of $f(u(t + \Delta t))$ is denoted by $-\eta f \Delta t \Delta s$:

$$-\eta f \Delta t \Delta s = \frac{f^T [\Delta u^\perp(t + \Delta t)]}{f^T f} f. \quad (\text{C.3})$$

$\Delta u^\perp(t + \Delta t)$ can be represented as the summation of its two orthogonal projections:

$$\Delta u^\perp(t) + (\partial_u f \Delta u^\perp(t) + \partial_s f \Delta s) \Delta t = \Delta u^\perp(t + \Delta t) - \eta f \Delta t \Delta s. \quad (\text{C.4})$$

recall our definition that $v = \Delta u / \Delta s$, $v^\perp = \Delta u^\perp / \Delta s$, and assume that Δt and Δs are infinitesimal, we obtain:

$$\frac{dv^\perp}{dt} = \partial_u f v^\perp + \partial_s f + \eta f. \quad (\text{C.5})$$

Here v is the tangent solution of Equation (5); v^\perp is the orthogonal projection of v according to Equation (9). Only η is unknown, so we can view Equation (C.5) as the definition of η .

We can show that:

$$\eta = -\frac{d\xi}{dt}. \quad (\text{C.6})$$

To see this, first Subtract Equation (C.5) from (5), we get:

$$\frac{d(v - v^\perp)}{dt} = \partial_u f(v - v^\perp) - \eta f. \quad (\text{C.7})$$

By our definition of ξ ,

$$\frac{d(\xi f)}{dt} = \partial_u f(\xi f) - \eta f. \quad (\text{C.8})$$

By Leibniz rule for differential,

$$\frac{d(\xi f)}{dt} = \xi \frac{df}{dt} + \frac{d\xi}{dt} f. \quad (\text{C.9})$$

Equation (C.6) is obtained by recalling the chain rule for differential,

$$\partial_u f(\xi f) = \xi \partial_u f(f) = \xi (\partial_u f \frac{du}{dt}) = \xi \frac{df}{dt}. \quad (\text{C.10})$$

To know the difference of the perturbed trajectory and the base trajectory, we need to define a correspondence between the states on the two trajectories. That is, we should know which state on one trajectory should be compared with

which state on the other trajectory. We want the corresponding states close to each other, which is essential for the next step derivation.

The first way is to compare the two trajectories at the same time frame. However, as we have seen in the left column of Figure 1, soon they will part from each other. This would make the higher order small quantities no longer negligible, hence our following analysis not working.

Alternatively, we can vary Δt so that the corresponding states of the two trajectories remain close. In time Δt , the new trajectory moves a length of $f\Delta t - \eta f\Delta t\Delta s$. So the new speed is $(1 - \eta\Delta s)f$. Hence the new trajectory needs time $\Delta t/(1 - \eta\Delta s) \approx \Delta t(1 + \eta\Delta s)$ to cross the same length $f\Delta t$. If we compare the point on base trajectory at time $(t + \Delta t)$ with the point on the perturbed trajectory at time $t + \Delta t(1 + \eta\Delta s)$, the distance is $\Delta u^\perp(t + \Delta t)$. Notice that $\Delta u^\perp(t) \approx v^\perp\Delta s$. Now if we have a v^\perp whose magnitude is small, then the corresponding Δu^\perp will always be in the same order of Δs .

The $J_{new}\Delta t_{new}$ on this small section of new trajectory is:

$$\begin{aligned} & J_{new}\Delta t_{new} \\ &= (J + \partial_u J \Delta u^\perp)(1 + \eta\Delta s)\Delta t \\ &= J\Delta t + \partial_u J \Delta u^\perp \Delta t + J\eta\Delta s\Delta t. \end{aligned} \quad (\text{C.11})$$

To compute the difference in averaged J , first write down its definition:

$$\begin{aligned} & \frac{1}{T_{new}} \int_0^{T_{new}} J_{new} dt - \frac{1}{T} \int_0^T J dt \\ &= \frac{1}{\int_0^T (1 + \eta\Delta s) dt} \int_0^T (J + \partial_u J \Delta u^\perp + J\eta\Delta s) dt - \frac{1}{T} \int_0^T J dt \\ &= \frac{\Delta s}{T} \int_0^T [\partial_u f v^\perp + \partial_s J + \eta(J - \langle J \rangle)] dt. \end{aligned} \quad (\text{C.12})$$

Let $\Delta s \rightarrow 0$, we have:

$$\frac{d}{ds} \left(\frac{1}{T} \int_0^T J dt \right) = \frac{1}{T} \int_0^T [\partial_u f v^\perp + \partial_s J + \eta(J - \langle J \rangle)] dt. \quad (\text{C.13})$$

First we use the shadowing direction v^∞ as v in above formula. Since $v^\infty(u)$ is uniformly bounded for all u on the attractor, the right hand side in Equation (C.13) converges uniformly as $T \rightarrow \infty$. This allows us to interchange the procedure of taking derivative with respect to s and letting T goes to infinity:

$$\begin{aligned} \frac{d}{ds} \langle J \rangle_\infty &= \frac{d}{ds} \left(\lim_{T \rightarrow \infty} \frac{1}{T} \int_0^T J dt \right) \\ &= \lim_{T \rightarrow \infty} \frac{1}{T} \int_0^T [\partial_u f v^\perp + \partial_s J + \eta(J - \langle J \rangle)] dt. \end{aligned} \quad (\text{C.14})$$

Here η is computed from Equation (C.5) by v^∞ . The mathematical proof that justifies the interchange of two procedures can be found in [24, 30].

If we use the NILSS solution v to approximate v^∞ , and use finite T , then we have the following approximation:

$$\frac{d\langle J \rangle_\infty}{ds} \approx \frac{1}{T} \int_0^T [\partial_u f v^\perp + \partial_s J + \eta(J - \langle J \rangle_T)] dt. \quad (\text{C.15})$$

Applying Equation (C.6), we can see this is exactly Equation (18).

From this deduction we can see why we want v^\perp to be small: our analysis requires neglecting higher order small quantities. If v^\perp grows exponentially, our analysis here is no longer valid.

Appendix D. Finite difference NILSS method

We can use finite difference results to approximate all the tangent solutions used in NILSS method. In fact, we only need to approximate v^* and W . Once their approximations are obtained, other parts of the algorithm follow.

To achieve this, first we compute a baseline primal solution u_b , which satisfies Equation (1) with initial condition u_0 . Here u_0 is an arbitrary state on the attractor.

To approximate v^* , we change s to $s + \Delta s$, and solve for u^* , which satisfies the perturbed governing equation with the same initial condition u_0 . Now we have:

$$v^* \approx \frac{u^* - u_b}{\Delta s}. \quad (\text{D.1})$$

To approximate homogeneous solution w with initial condition w_0 , we first scale w_0 by ϵ , such that ϵw_0 is small. Then solve for u^w by keeping the same s but using initial conditions $u_0 + \epsilon w_0$. The approximation for w is:

$$w \approx \frac{u^w - u_b}{\epsilon}. \quad (\text{D.2})$$

The benefit of this finite difference version of NILSS is that it is truly non-intrusive. In fact, it even no longer requires a tangent solver, all it needs is a simulation software which can solve for the primal solution.

The downside is that, the approximation by finite difference may incur additional error. Also, when deciding the time segment length ΔT , there is an extra requirement, that is, the perturbation do not grow too large. Otherwise, the perturbation may fall out of the linear region, and the finite difference no longer approximates the tangent solution.

Appendix E. Derivation of $d\langle J \rangle_\infty/ds$ on multiple segments

To derive Equation (44) from Equation (18), first we recover a continuous tangent solution v from $\{v_i^\perp\}$ on each segment and ξ ‘accumulated’ from all previous segments:

$$v(t) = v^\perp(t) + \xi(t)f(t), \quad (\text{E.1})$$

where

$$\begin{cases} v^\perp(t) = v_i^\perp(t), \\ \xi(t) = \xi_i(t) + \sum_{i'=0}^{i-1} \xi_{i'}(t_{i'+1}), \end{cases} \quad t \in [t_i, t_{i+1}], \quad (\text{E.2})$$

where $\{v_i^\perp(t)\}$ are given by Equation (41), $\xi_i(t)$ are given by Equation (42).

The continuity of v follows from the continuity of v^\perp and ξ . $v^\perp(t)$ is continuous because of the continuity condition in Equation (38). $\xi(t)$ is continuous because $\xi_i(t_i) = 0$, as shown in Equation (43).

To see that v is a tangent solution of Equation (5), first notice that on segment i ,

$$v(t) = v_i(t) + \xi_i^* f(t), \quad t \in [t_i, t_{i+1}], \quad (\text{E.3})$$

where $\xi_i^* = \sum_{i'=0}^{i-1} \xi_{i'}(t_{i'+1})$. Take time derivative of v , we have:

$$\begin{aligned} \frac{dv}{dt} &= \frac{dv_i}{dt} + \xi_i^* \frac{df}{dt} = \partial_u f v_i + \partial_s f + \xi_i^* \partial_u f f \\ &= \partial_u f (v_i + \xi_i^* f) + \partial_s f = \partial_u f v + \partial_s f. \end{aligned} \quad (\text{E.4})$$

To conclude, v is a continuous tangent solution on the entire trajectory, whose v^\perp is small. By applying Equation (18) to v , we obtain Equation (44).

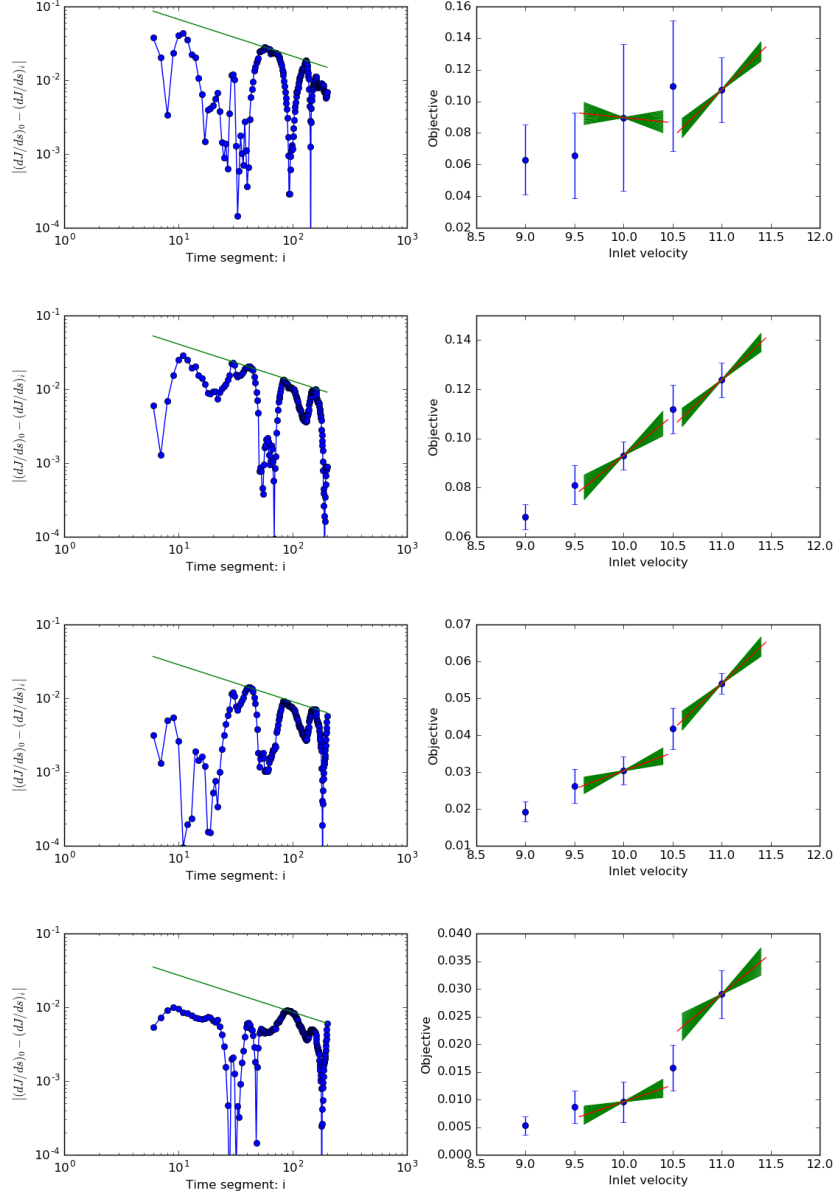


Figure 10: Sensitivity computed by NILSS. From top to bottom the objective function is the long-time average of $U_x/10$, $(U_x/10)^2$, $(U_x/10)^4$, and $(U_x/10)^8$. Left column: sensitivity computed by increasing number of segments, the lines indicates confidence intervals for sensitivities. Right column: sensitivity plotted with objectives for adjacent parameters, the bars and wedges indicate confidence intervals of the objectives and sensitivities, respectively.

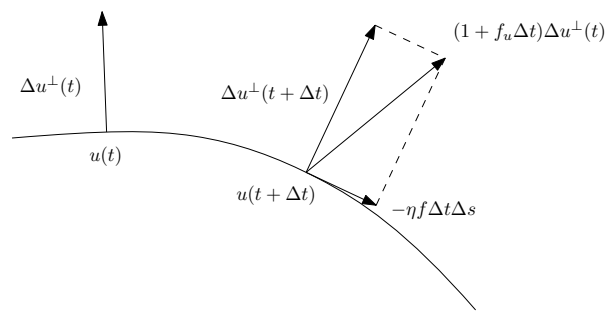


Figure C.11: Perturbation of the trajectory due to perturbation on the parameter.